

Spatiotemporal Transformers for Predicting Avian Disease Risk from Migration Trajectories

Dingya Feng Dingyuan Xue
1947379538@qq.com xuedy@uw.edu

ABSTRACT

Accurate forecasting of avian disease outbreaks is critical for wildlife conservation and public health. This study presents a Transformer-based framework for predicting the disease risk at the terminal locations of migratory bird trajectories. We integrate multi-source datasets, including GPS tracking data from Movebank, outbreak records from the World Organisation for Animal Health (WOAH), and geospatial context from GADM and Natural Earth. The raw coordinates are processed using H3 hierarchical geospatial encoding to capture spatial patterns. The model learns spatiotemporal dependencies from bird movement sequences to estimate endpoint disease risk. Evaluation on a held-out test set demonstrates strong predictive performance, achieving an accuracy of 0.9821, area under the ROC curve (AUC) of 0.9803, average precision (AP) of 0.9299, and an F1-score of 0.8836 at the optimal threshold. These results highlight the potential of Transformer architectures to support early-warning systems for avian disease surveillance, enabling timely intervention and prevention strategies.

Introduction

Avian-borne pathogens pose persistent risks to wildlife and, at times, to public health; the ongoing H5N1 panzootic has caused extensive mortality in wild birds and livestock with continued geographic expansion and zoonotic concern (Mostafa et al., 2025). Migratory birds link distant ecosystems across seasons and can create spatiotemporal pathways for pathogen dispersal, with phylodynamic and migration evidence supporting long-range movements of HPAI along flyways, including documented trans-Atlantic incursion events (Banyard et al., 2024).

Operational early-warning and risk assessment commonly rely on outbreak notifications and targeted surveillance (e.g., WOAH's WAHIS Early Warning), often paired with mathematical or statistical models. Classic global modeling integrated bird flyways, phylogenies, and trade to forecast international spread of H5N1 and identify invasion pathways (Kilpatrick et al., 2006). Recent genomic and phylodynamic analyses further link dispersal patterns to migration timing and characterize post-introduction spread across flyways (Nguyen et al., 2025; Yang et al., 2024). Telemetry-informed contagion modeling has combined multi-year GPS tracks of migratory waterfowl with county-level detections to forecast H5N1 spread, offering advance warning for wildlife (McDuiie et al., 2024). In parallel, machine-learning studies have mapped risk using environmental and agro-ecological covariates rather than individual movement sequences: Random Forests produced a global AIV risk map for wild birds; boosted regression trees mapped H5N1 risk from poultry density, human density, and elevation; and gradient-boosted learners achieved daily, premises-level risk estimation during epidemics (Herrick et al., 2013; Martin et al., 2011; Yoo et al., 2022). However, these tools typically operate on static grids or aggregated predictors and do not learn directly from fine-scale telemetry. To our knowledge, there are no peer-reviewed studies that train sequence-learning neural networks (e.g., Transformers) on individual GPS migration trajectories to predict endpoint disease risk; our work addresses this gap by ingesting full trajectories, encoding space with hierarchical H3 cells, and training a Transformer(Vaswani et al., 2017) to estimate endpoint risk.

Here we assemble a multi-source dataset that links GPS tracking data from Movebank with officially reported outbreak records from WOAH, and augments each trajectory with administrative and physical context from GADM and Natural Earth. Locations are encoded with hierarchical H3 (*Uber/H3*, 2017/2025) cells to capture spatial structure at multiple scales, and the model consumes full migration trajectories to produce an endpoint disease risk score. On a held-out test set, the Transformer achieves high performance (AP = 0.929); using a validation-selected decision threshold ($t = 0.992$), it attains F1 = 0.8836. These results suggest that learning directly from high-resolution movement sequences can complement existing surveillance by flagging high-risk endpoints for targeted monitoring and prevention.

Methods

Dataset

Bird migration telemetry (Movebank). We compiled GPS/GSM tracking data from publicly downloadable datasets on Movebank (*Movebank*, n.d.), selecting 11 datasets that cover 7 representative species spanning ducks and geese (Anseriformes), the best-supported wild-bird reservoirs for influenza A. Species selection followed Movebank data availability and guidance from Olson (Olsen et al., 2006), who reviewed host groups most frequently implicated in avian influenza maintenance and identified Anseriformes (ducks, geese, swans) as the primary natural hosts. The telemetry corpus totals ~4.7 million GPS fixes from 552 individuals without duplication (see Table S1 for datasets and species).

Table 1. Movebank studies used in this work

Group	Species	Movebank study name	Individuals (n)
Duck	Anas platyrhynchos	MPIAB Lake Constance Mallards GPS(Korner et al., 2016)	52
Duck	Anas platyrhynchos	Navigation and migration in European mallards(Van Toor et al., 2013)	68
Duck	Anas crecca	Eurasian teal, Giunchi, Italy(Cerritelli et al., 2023)	47
Duck	Anas acuta	northernPintail_USGS_ASC_argos(Jerry W Hupp et al., 2019)	129
Duck	Anas discors	blueWingedTeal_USGS_ASC_argos(Andy M Ramey et al., 2019)	42
Geese	Anser albifrons	Migration timing in white-fronted geese(Kölzsch, Kruckenberg, et al., 2016)	65
Geese	Anser albifrons	North Sea population tracks of greater white-fronted geese(Kölzsch et al., 2019)	81
Geese	Anser albifrons	White-fronted goose full year tracks 2006-2010 Alterra IWWR(Kölzsch, Müskens, et al., 2016)	7
Geese	Anser anser	Graugans Zugverhalten Neusiedler See(Grabenhofer, 2025)	30
Geese	Branta canadensis	North-East American Canada goose migration 2015-2021(Sorais, 2021)	82

Outbreak records (WOAH/WAHIS). Global animal-health events were obtained from the World Organisation for Animal Health (WOAH) – WAHIS platform (*WAHIS*, n.d.). We retained all records tagged to poultry and wild-bird hosts for avian-related diseases. Event metadata were used downstream for spatiotemporal joins.

Administrative boundaries (GADM). To link point tracks and outbreaks within comparable geopolitical units, we downloaded global administrative polygons from GADM (*GADM*, n.d.) and assigned each GPS fix and outbreak record to level-1/2 units via point-in-polygon joins.

Physical geography (Natural Earth). Because avian influenza ecology is tightly coupled to aquatic habitats used by waterfowl (Martin et al., 2011), we overlaid tracks on Natural Earth (*Natural Earth - Free Vector and Raster Map Data at 1*, n.d.) physical layers and classified each fix into lake, land, or ocean using lake polygons, land/ocean polygons.

Integrated disease–movement table. Finally, we merged the telemetry and outbreak layers by administrative unit and date, producing a per-fix table that pairs each trajectory point with (i) its terrain and (ii) any contemporaneous avian-disease events in that unit within two weeks.

Dataset Processing

We first resampled each individual's track to a 12-hour interval to standardize timing and then segmented the series into 30-day windows. For each window, we built step-level continuous features x_cont with shape $T \times 14$ (where T is the number of 12-hour steps in 30 days). The 14 features include: (i) 3D unit-sphere coordinates transformed from latitude/longitude (x , y , z) as **Equation 1**, (ii) great-circle step distance and derived speed as **Equation 2** (iii) movement direction encoded as sin/cos of bearing as **Equation 3**, (iv) diurnal and seasonal phase (hour-of-day and day-of-year encoded as sin/cos), and (v) a one-hot terrain indicator for land/lake/ocean.

Equation 1: Spherical coordinates to 3D unit sphere (x, y, z ; 3 dims in x_cont):

Let $\{(\varphi_t, \lambda_t)\}_{t=1}^T$ be latitude/longitude (in radians)

$$x_t = \cos \varphi_t \cos \lambda_t, y_t = \cos \varphi_t \sin \lambda_t, z_t = \sin \varphi_t.$$

Equation 2: Step length and speed (d_t, v_t ; 2 dims in x_cont):

$$a_t = \sin^2\left(\frac{\Delta\varphi_t}{2}\right) + \cos \varphi_{t-1} \cos \varphi_t \sin^2\left(\frac{\Delta\lambda_t}{2}\right), d_t = 2R \arcsin(\sqrt{a_t}), v_t = \frac{d_t}{\Delta t}.$$

Equation 3: Bearing (encoded as $\sin \theta_t, \cos \theta_t$; 2 dims in x_cont):

$$\Delta\lambda_t = \lambda_t - \lambda_{t-1}, \theta_t = \tan^{-1}\left(\frac{\sin(\Delta\lambda_t) \cos(\varphi_t)}{\cos(\varphi_{t-1}) \sin(\varphi_t) - \sin(\varphi_{t-1}) \cos(\varphi_t) \cos(\Delta\lambda_t)}\right)$$

We map each fix from geographic coordinates to an H3 index at a fixed resolution to represent location. Compared with raw latitude/longitude, H3’s hexagonal, hierarchical grid offers (i) consistent, locality-preserving cell adjacencies, (ii) straightforward multi-resolution aggregation, and (iii) simpler neighborhood operations (rings/k-nearest cells), which together reduce distortions that arise when binning or modeling on raw lat/long (Bousquin, 2021).

To summarize longer-term movement context beyond the 30-day window, we compute an 18-dimensional context vector (ctx_vec) from recent history. It aggregates high-level mobility statistics (e.g., cumulative distance, straight-line displacement, tortuosity, unique H3 cells visited, average speed), seasonal/temporal encodings, and terrain composition over the historical period, providing the model with coarse priors about an individual’s recent behavior and habitat use.

We apply two lightweight masks to suppress unnecessary information during training: a padding mask that hides padded steps inside windows and an observation mask that hides steps without actual telemetry. Finally, each window receives a binary label based on the endpoint’s epidemiological status—positive if a WOAH-recorded avian-disease event occurs in the endpoint’s administrative unit (or corresponding H3 cell) within a fixed post-endpoint time horizon (14 days), and negative otherwise.

Model Training

We train on the processed windows described above—each sample provides step-level features x_cont , an $H3$ sequence, a *species ID*, a history context vector ctx_vec , and two masks (padding/observation). The backbone is a Transformer encoder. Per step, we project x_cont to the model width and add (i) a projected $H3$ embedding and (ii) sinusoidal positional encoding; a species embedding is added as a per-step bias. We also prepend a learned $[CTX]$ token formed by an MLP over ctx_vec plus the species embedding. In PyTorch (Paszke et al., 2019), the encoder is a pre-norm *nn.TransformerEncoder* (e.g., six layers, six heads, dropout 0.15). A key-padding mask hides padded steps; the window-level logit is read from the last valid step (indexing accounts for the prepended $[CTX]$). Optionally, the model also emits per-step logits for an auxiliary loss.

Optimization follows standard binary classification practice with class imbalance handling. We train with *BCEWithLogitsLoss* using a *pos_weight* computed from the train labels; additionally, the *DataLoader* can oversample positives (weight 3.0). We use *AdamW* (learning rate 2×10^{-4}), weight decay 10^{-4} , mixed-precision (AMP), and gradient clipping (1.0). We save the best-AP checkpoint. After training, we select a decision threshold on the validation set by maximizing F1 and then report test metrics at that fixed threshold. To prevent leakage from near-duplicate endpoints, we use a grouped cohort split: *species* \times *destination* \times *year-week* defines a cohort, and cohorts are assigned exclusively to **train**/**val**/**test**. The whole process is shown in Figure 1.

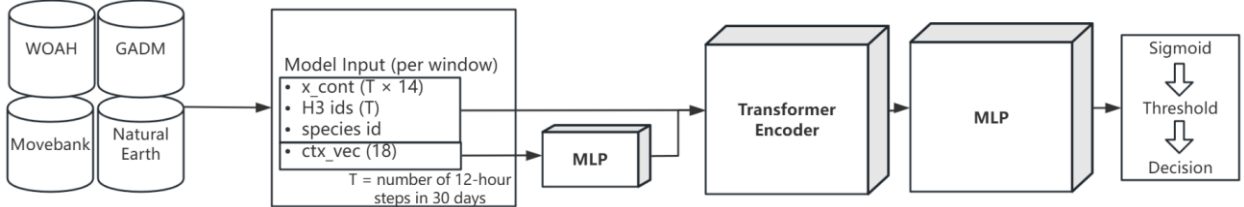


Figure 1. Spatiotemporal Pipeline for Migration-Based Disease Risk Prediction.

Results

Our transformer-based spatiotemporal model achieved consistently strong predictive performance across training, validation, and independent test sets. Figure 2 illustrates the training and validation loss curves over 30 epochs, with the best model obtained at epoch 17, where the training loss reached 0.0392 and the validation loss reached 0.1777. At this point, validation metrics were high (accuracy = 0.9711, AUC = 0.9767, AP = 0.9039). When evaluated on the held-out test set, the model achieved an accuracy of 0.9821, AUC of 0.9803, AP of 0.9299, and an F1-score of 0.884 at the optimal threshold (0.992) selected from the validation set (Figure 3).

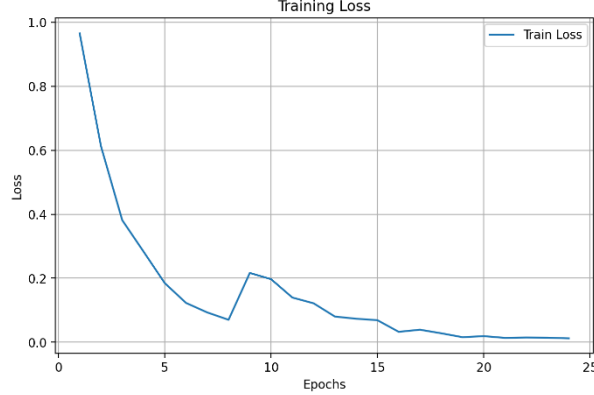


Figure 2. Training and validation loss curves over 30 epochs.

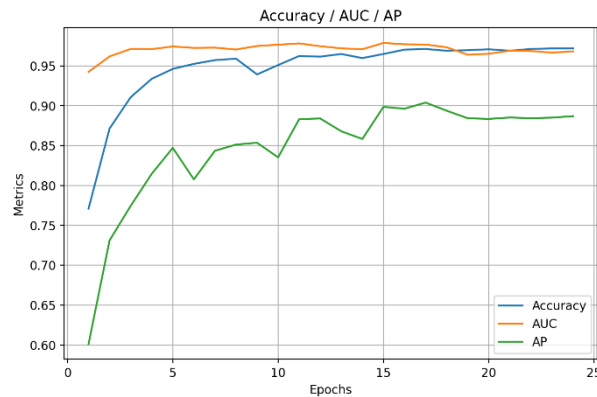


Figure 3. Performance metrics on the held-out test set. The best model achieved 0.9821 accuracy, 0.9803 Area Under ROC (AUC), 0.9299 Average Precision (AP)

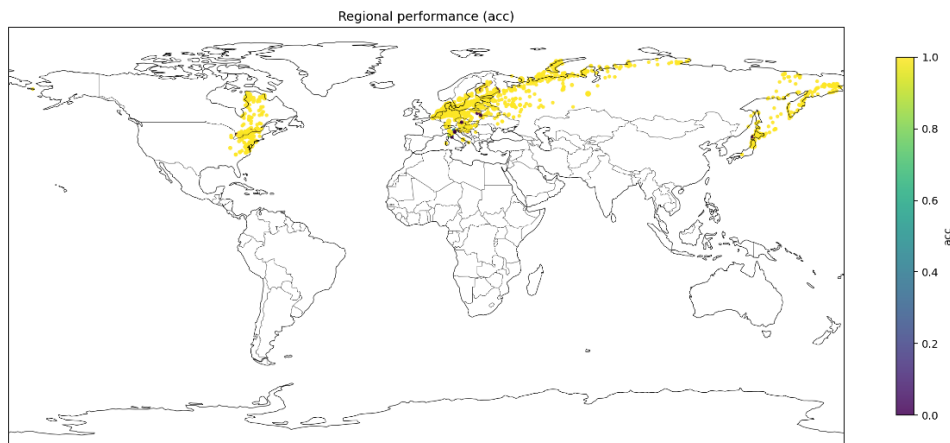


Figure 4. Regional accuracy map. Model predictions were accurate across all geographic regions in the test set, indicating strong spatial generalization.

Spatial generalization was also strong: Figure 4 shows per-region accuracy, with all regions exhibiting high predictive performance, suggesting that the model captures generalizable spatiotemporal risk patterns rather than overfitting to specific localities.

We further examined performance across bird species (Table 2), finding that the model maintained high accuracy for all target species, with minor variation likely due to sample size and movement ecology differences.

Table 2. Per-species prediction accuracy. Accuracy values are reported for each of the seven target species, showing robust performance across different hosts.

Species	Accuracy	AUC	AP	F1-score
Anser brachyrhynchus	0.999	0.999	0.999	0.999
Anser albifrons	0.998	0.997	0.977	0.975
Anas acuta	0.998	1.000	1.000	0.933
Anas platyrhynchos	0.996	1.000	1.000	0.947
Branta leucopsis	0.994	0.978	0.943	0.925
Branta canadensis	0.985	0.997	0.991	0.980
Anser fabalis	0.967	0.857	0.370	0.235
Anser anser	0.963	0.967	0.619	0.731
Anas crecca	0.914	0.893	0.682	0.677

To contextualize our approach, we selected two representative baselines from prior avian influenza risk prediction studies. The first is the work of Fang et al. (Martin et al., 2011), which developed logistic regression and boosted regression tree (BRT) models to predict the presence of HPAI H5N1 in China using outbreak records and risk-based surveillance data. These models incorporated environmental, host, and anthropogenic covariates but did not explicitly leverage high-resolution movement trajectories. Their reported evaluation AUC values ranged from 0.864 (logistic regression, outbreak data) to 0.967 (BRT, surveillance data). The second is the global ecological niche model of Hill et al. (Herrick et al., 2013), which employed a random forest classifier trained on environmental predictors to estimate the relative occurrence of avian influenza viruses in wild birds worldwide, achieving an AUC of 0.760 on independent test points.

Table 3 shows that on our 0–14 day endpoint prediction task, the proposed Transformer-based sequence model achieved an AUC of 0.980, surpassing all baseline values, underscoring the benefit of incorporating fine-grained movement trajectories, spatial encoding, and temporal context into a unified sequence-learning framework.

Table 3. Comparison with baseline methods. Overall predictive performance of our transformer-based model compared with adapted baselines from prior avian influenza risk models.

Method	AUC
Logistic Regression (Outbreak)	0.864
Logistic Regression (Surveillance)	0.900
BRT (Outbreak)	0.940
BRT (Surveillance)	0.967
Random Forest (Veterinary Research)	0.760
Ours	0.980

Discussion

The strong predictive performance of our model is consistent with expectations, given the combination of a modern Transformer-based architecture and the use of fine-grained bird migration trajectories enriched with multi-dimensional spatiotemporal features. By jointly encoding step-level movement information, spatial context through H3 geocoding, and aggregated historical context vectors, the model can capture complex patterns inaccessible to simpler modeling approaches or static environmental predictors alone. The strong predictive performance of our model is consistent with expectations, given the combination of a modern Transformer-based architecture and the use of fine-grained bird

migration trajectories enriched with multi-dimensional spatiotemporal features. By jointly encoding step-level movement information, spatial context through H3 geocoding, and aggregated historical context vectors, the model can capture complex patterns inaccessible to simpler modeling approaches or static environmental predictors alone.

Spatially, model performance was uniformly high across most regions, with minor variability observed in certain areas of Europe. This outcome is unsurprising and likely reflects dataset incompleteness. The Movebank platform offers only a limited number of publicly downloadable datasets; in this study, we were able to use just 11 migration datasets, with the majority of records concentrated in Europe and North America. Consequently, even within these continents, the available data cannot fully cover the entire geographic range, and data density varies across subregions. Performance fluctuations may occur if certain areas have distinct movement or ecological characteristics. Regions outside Europe and North America remain largely data-sparse or absent, and model performance is expected to degrade sharply when applied to such areas. Expanding coverage with more geographically diverse datasets would be an important step toward improving global generalizability.

Species-level performance differences are also consistent with expectations. For several species, available records derive from a single study, leading to both a limited sample size and reduced ecological diversity in their trajectories. Such constraints inevitably limit the ability of the model to learn robust, transferable risk signatures for those hosts.

Our model's performance advantage is substantial when compared with established baselines from the avian influenza modeling literature. Although these baseline methods—logistic regression, boosted regression trees, and ecological niche modeling via random forests—were not designed to forecast disease presence within a specific short-term horizon, they represent well-recognized approaches for mapping avian influenza risk. Our substantially higher AUC demonstrates not only the utility of our approach for the 0–14 day endpoint prediction task but also its novelty: integrating detailed spatiotemporal movement data of migratory birds with advanced sequence-learning techniques to directly anticipate outbreak risk in the near future. This framing opens a new direction for wildlife disease early warning systems, where movement ecology is operationally fused with predictive modeling.

Conclusion

In this study, we developed a Transformer-based sequence modeling framework to predict the risk of avian disease outbreaks within 14 days at the terminal point of migratory bird trajectories. Leveraging high-resolution movement data from Movebank, integrated with spatial context via H3 geocoding, administrative boundaries from GADM, outbreak records from WOAH, and terrain information from Natural Earth, our approach captures complex spatiotemporal dependencies that static models cannot. The model achieved state-of-the-art predictive performance on held-out test data, with an AUC of 0.980, substantially exceeding established baselines from the avian influenza risk modeling literature.

Our innovation lies in directly integrating fine-grained migratory trajectories with multi-scale spatial encoding and temporal context to forecast short-horizon outbreak risk, bridging movement ecology and disease early-warning systems. While traditional ecological niche or statistical risk models provide static probability maps, our framework operationalizes continuous telemetry into actionable, time-bound predictions. This capability has direct implications for wildlife disease surveillance and could be extended to other migratory species or pathogen systems.

Future work will focus on expanding the spatial and temporal coverage of migration datasets, incorporating more detailed environmental variables, and validating the model in operational early-warning contexts. With richer and more diverse data, this approach holds promise for improving global preparedness and response to emerging wildlife-borne diseases.

Limitations

The primary limitation of this study lies in the scope and diversity of the available datasets. For each target bird species, more records are needed from multiple independent studies that capture movements across a wider range of geographic regions and ecological contexts. Temporal coverage should also be expanded: for individual migration routes, having data from multiple years would allow the model to account for interannual variability in movement patterns and disease dynamics. In terms of dataset construction, our habitat representation was constrained by the Natural Earth dataset, from which only three coarse terrain categories—lake, land, and ocean—were incorporated. Other landscape features known to influence migratory bird behavior, such as rivers, mountain ranges, and wetlands,

were not included. Incorporating such fine-scale environmental attributes in future work could further enhance model accuracy and ecological realism.

Acknowledgements

We thank the researchers and institutions who contributed migration tracking data to the Movebank Data Repository, making their work publicly available for scientific use. These datasets provided the essential foundation for this study and reflect the collaborative effort of the movement ecology community to advance open science.

References

Andy M Ramey, C. Soos, P. Link, P. Walther, Lee Tibbitts, & David C Douglas. (2019). *Tracking Data for Blue-winged Teal (Anas discors)* [Zip, csv]. U.S. Geological Survey. <https://doi.org/10.5066/P9Z9BA9F>

Banyard, A. C., Bennison, A., Byrne, A. M. P., Reid, S. M., Lynton-Jenkins, J. G., Mollett, B., De Silva, D., Peers-Dent, J., Finlayson, K., Hall, R., Blockley, F., Blyth, M., Falchieri, M., Fowler, Z., Fitzcharles, E. M., Brown, I. H., & James, J. (2024). Detection and spread of high pathogenicity avian influenza virus H5N1 in the Antarctic Region. *Nature Communications*, 15(1), 7433. <https://doi.org/10.1038/s41467-024-51490-8>

Bousquin, J. (2021). Discrete Global Grid Systems as scalable geospatial frameworks for characterizing coastal environments. *Environmental Modelling & Software : With Environment Data News*, 146, 1–14. <https://doi.org/10.1016/j.envsoft.2021.105210>

Cerritelli, G., Vanni, L., Baldaccini, N. E., Lenzoni, A., Sorrenti, M., & Giunchi, D. (2023). Trailing the heat: Eurasian teal *Anas crecca* schedule their spring migration basing on the increase in soil temperatures along the route. *Journal of Avian Biology*, 2023(9–10), e03122. <https://doi.org/10.1111/jav.03122>

GADM. (n.d.). Retrieved August 12, 2025, from <https://gadm.org/>

Grabenhofer, H. (2025). *Graugans Zugverhalten Neusiedler See* [Csv]. https://www.movebank.org/cms/webapp?gwt_fragment=page=studies,path=study505156776

Herrick, K. A., Huettmann, F., & Lindgren, M. A. (2013). A global model of avian influenza prediction in wild birds: The importance of northern regions. *Veterinary Research*, 44(1), 42. <https://doi.org/10.1186/1297-9716-44-42>

Jerry W Hupp, Lee Tibbitts, & David C Douglas. (2019). *Tracking Data for Northern Pintails (Anas acuta)* [Csv]. U.S. Geological Survey. <https://doi.org/10.5066/P90A6HW3>

Kilpatrick, A. M., Chmura, A. A., Gibbons, D. W., Fleischer, R. C., Marra, P. P., & Daszak, P. (2006). Predicting the global spread of H5N1 avian influenza. *Proceedings of the National Academy of Sciences*, 103(51), 19368–19373. <https://doi.org/10.1073/pnas.0609227103>

Kölzsch, A., Kruckenberg, H., Glazov, P., Müskens, G. J. D. M., & Wikelski, M. (2016). *Data from: Towards a new understanding of migration timing: slower spring than autumn migration in geese reflects different decision rules for stopover use and departure* [Dataset]. Movebank Data Repository. <https://doi.org/10.5441/001/1.31C2V92F>

Kölzsch, A., Müskens, G. J. D. M., Kruckenberg, H., Glazov, P., Weinzierl, R., Nolet, B. A., & Wikelski, M. (2016). Towards a new understanding of migration timing: Slower spring than autumn migration in geese reflects different decision rules for stopover use and departure. *Oikos*, 125(10), 1496–1507. <https://doi.org/10.1111/oik.03121>

Kölzsch, A., Müskens, G. J. D. M., Moonen, S., Kruckenberg, H., Glazov, P., & Wikelski, M. (2019). *Data from: Flyway connectivity and exchange primarily driven by moult migration in geese [North Sea population]* [Dataset]. Movebank Data Repository. <https://doi.org/10.5441/001/1.CT72M82N>

Korner, P., Sauter, A., Fiedler, W., & Jenni, L. (2016). Variable allocation of activity to daylight and night in the mallard. *Animal Behaviour*, 115, 69–79. <https://doi.org/10.1016/j.anbehav.2016.02.026>

Martin, V., Pfeiffer, D. U., Zhou, X., Xiao, X., Prosser, D. J., Guo, F., & Gilbert, M. (2011). Spatial Distribution and Risk Factors of Highly Pathogenic Avian Influenza (HPAI) H5N1 in China. *PLOS Pathogens*, 7(3), e1001308. <https://doi.org/10.1371/journal.ppat.1001308>

McDuiie, F., T. Overton, C., A. Lorenz, A., L. Matchett, E., L. Mott, A., A. Mackell, D., T. Ackerman, J., De La Cruz, S. E. W., Patil, V. P., Prosser, D. J., Takekawa, J. Y., Orthmeyer, D. L., Pitesky, M. E., Díaz-Muñoz, S. L., Riggs, B. M., Gendreau, J., Reed, E. T., Petrie, M. J., Williams, C. K., ... Casazza, M. L. (2024). Mitigating Risk: Predicting H5N1 Avian Influenza Spread with an Empirical Model of Bird Movement. *Transboundary and Emerging Diseases*, 2024, 5525298. <https://doi.org/10.1155/2024/5525298>

Mostafa, A., Nogales, A., & Martinez-Sobrido, L. (2025). Highly pathogenic avian influenza H5N1 in the United States: Recent incursions and spillover to cattle. *Npj Viruses*, 3(1), 54. <https://doi.org/10.1038/s44298-025-00138-5>

Movebank. (n.d.). Retrieved August 12, 2025, from <https://www.movebank.org/cms/movebank-main>

Natural Earth—Free vector and raster map data at 1:10m, 1:50m, and 1:110m scales. (n.d.). Retrieved August 12, 2025, from <https://www.naturalearthdata.com/>

Nguyen, T.-Q., Hutter, C. R., Markin, A., Thomas, M., Lantz, K., Killian, M. L., Janzen, G. M., Vijendran, S., Wagle, S., Inderski, B., Magstadt, D. R., Li, G., Diel, D. G., Frye, E. A., Dimitrov, K. M., Swinford, A. K., Thompson, A. C., Snekvik, K. R., Suarez, D. L., ... Anderson, T. K. (2025). Emergence and interstate spread of highly pathogenic avian influenza A(H5N1) in dairy cattle in the United States. *Science*, 388(6745), eadq0900. <https://doi.org/10.1126/science.adq0900>

Olsen, B., Munster, V. J., Wallensten, A., Waldenström, J., Osterhaus, A. D. M. E., & Fouchier, R. A. M. (2006). Global Patterns of Influenza A Virus in Wild Birds. *Science*, 312(5772), 384–388. <https://doi.org/10.1126/science.1122438>

Paszke, A., Gross, S., Massa, F., Lerer, A., Bradbury, J., Chanan, G., Killeen, T., Lin, Z., Gimelshein, N., Antiga, L., Desmaison, A., Kopf, A., Yang, E., DeVito, Z., Raison, M., Tejani, A., Chilamkurthy, S., Steiner, B., Fang, L., ... Chintala, S. (2019). *PyTorch: An Imperative Style, High-Performance Deep Learning Library* (No. arXiv:1912.01703). arXiv. <https://doi.org/10.48550/arXiv.1912.01703>

Sorais, M. (2021). *North-East American Canada goose migration 2015-2021* [Csv].

https://www.movebank.org/cms/webapp?gwt_fragment=page=studies,path=study2105214573

Uber/h3. (2025). [C]. Uber Open Source. <https://github.com/uber/h3> (Original work published 2017)

Van Toor, M. L., Hedenström, A., Waldenström, J., Fiedler, W., Holland, R. A., Thorup, K., & Wikelski, M. (2013). Flexibility of Continental Navigation and Migration in European Mallards. *PLoS ONE*, 8(8), e72629. <https://doi.org/10.1371/journal.pone.0072629>

Vaswani, A., Shazeer, N., Parmar, N., Uszkoreit, J., Jones, L., Gomez, A. N., Kaiser, Ł., & Polosukhin, I. (2017). Attention is all you need. *Proceedings of the 31st International Conference on Neural Information Processing Systems*, 6000–6010.

WAHIS. (n.d.). Retrieved August 12, 2025, from <https://wahis.woah.org/#/home>

Yang, Q., Wang, B., Lemey, P., Dong, L., Mu, T., Wiebe, R. A., Guo, F., Trovão, N. S., Park, S. W., Lewis, N., Tsui, J. L.-H., Bajaj, S., Cheng, Y., Yang, L., Haba, Y., Li, B., Zhang, G., Pybus, O. G., Tian, H., & Grenfell, B. (2024). Synchrony of Bird Migration with Global Dispersal of Avian Influenza Reveals Exposed Bird Orders. *Nature Communications*, 15(1), 1126. <https://doi.org/10.1038/s41467-024-45462-1>

Yoo, D., Song, Y., Choi, D., Lim, J.-S., Lee, K., & Kang, T. (2022). Machine learning-driven dynamic risk prediction for highly pathogenic avian influenza at poultry farms in Republic of Korea: Daily risk

estimation for individual premises. *Transboundary and Emerging Diseases*, 69(5), 2667–2681.

<https://doi.org/10.1111/tbed.14419>